

# UNSTEADY TWO-DIMENSIONAL FLOW RECONSTRUCTION AND FORCE COEFFICIENT ESTIMATION AROUND ARBITRARY SHAPES VIA CONFORMAL MAPPING AIDED DEEP NEURAL NETWORKS

Ali Girayhan Özbay

Turbulence Simulation Group  
Department of Aeronautics  
Imperial College London  
London SW7 2AZ, UK  
aligirayhan.ozbay14@imperial.ac.uk

Sylvain Laizet

Turbulence Simulation Group  
Department of Aeronautics  
Imperial College London  
London SW7 2AZ, UK  
s.laizet@imperial.ac.uk

## ABSTRACT

In many practical fluid dynamics experiments, measuring variables such as velocity and pressure is possible only at a limited number of sensor locations. However, knowledge of the full fields is necessary to understand the dynamics of many flows. Deep learning reconstruction of full flow fields from sparse measurements as a way of overcoming this limitation has recently garnered significant research interest, referred to as the flow reconstruction (FR) task.

We extend existing FR models by enabling such models to make predictions on flows around arbitrary 2D geometries without the need for re-training. This geometry flexibility is achieved through an innovative mapping approach, whereby multiple fluid domains are mapped to an annulus.

Using this mapping approach, we explore the performance of a novel FR model trained on 64 geometries and tested on a further 16 different geometries. We demonstrate that the model trained using the mapping approach reconstructs the flow fields well even on geometries not present in the training data.

## INTRODUCTION

Flow reconstruction (FR) involves the prediction of dense fields such as velocity based on sparse measurements. Though the usage of various statistical methods for this purpose has a long history in works such as Bonnet *et al.* (1994); Callahan *et al.* (2019). Recent advancements in deep learning (DL) rekindled an interest in flow reconstruction as seen in recent works such as Erichson *et al.* (2020); Dubois *et al.* (2022).

One drawback even in the recent DL based approaches is the necessity to train on the same geometry on which inference is to be performed. This inhibits the usefulness of FR models in practical scenarios, for instance in physical wind tunnel testing driven shape optimization. Overcoming this requires FR models that are capable of handling arbitrary geometries. Augmenting the training dataset with different geometries is not a solution for existing models such as the Shallow Decoder (SD) by Erichson *et al.* (2020), as our experimentation revealed that training the SD on a dataset with different geometries leads to a model that erroneously predicts fields that are averaged across all geometries in the dataset.

Sidestepping this issue is possible by representing the flow field in a way that removes the necessity to predict the physical geometry of the object in the fluid flow. However,

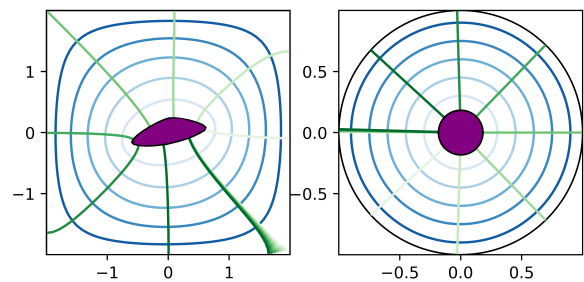


Figure 1: A random geometry (left) and its preimage in the  $w$  domain (right). Blue and green contours depict the norm and argument in the  $w$  domain, respectively.

only one work in previous literature investigates this avenue; Chen *et al.* (2021) used graph convolutional neural networks (GCNNs) to reconstruct laminar, steady pressure and velocity fields around random geometries at a low Reynolds number ( $Re = 10$ ). An alternate to GCNNs is the usage of a mapping, ensuring all geometries are mapped to a single shape. In 2D, this can be achieved through a Schwarz-Christoffel (S-C) conformal mapping; each  $k$ -connected region can be mapped to a disc with  $k$  holes, as explored by Crowdy (2020).

In this work, we explore doubly connected S-C mappings to generate datasets for training of FR models on large numbers of geometries, targeting reconstruction in space and time. Figure 1 depicts an example mapping for a geometry used in this study. Using this approach, we extend the capabilities demonstrated by Chen *et al.* (2021), investigating unsteady reconstruction at a much higher Reynolds number  $Re = 300$ .

As a further remark, for readers who are interested in the mapping strategy, our previous paper on the subject (Özbay & Laizet (2022)) covers the subject in greater detail. The present work builds upon the results in the results in the previous paper, extending them by adding an investigation of lift and drag prediction.

## DATA AND EXPERIMENTAL SETUP

Our dataset consists of 80 geometries  $G_i, i \in [0, 79]$ , randomly generated using Bezier curves using the code provided by Viquerat *et al.* (2021). The control points of the Bezier curves were chosen randomly in a square domain with charac-

teristic length  $L_m$ . Each geometry was placed in the center of a  $40L_m/3 \times 40L_m/3$  square domain, on the edges of which a uniform  $(u, v) = (1.0, 0.0)$  velocity Dirichlet BC was imposed. The flow around each  $G_i$  was computed at  $Re = uL_m/\nu = 300$  with the `PYFR` solver by Witherden *et al.* (2014). 600 snapshots between times  $\tau^* = 3.333$  and  $\tau^* = 23.333$  were recorded per geometry, where  $\tau^* = u\tau/L_m$  and  $\tau$  is the physical time.

Subsequently, denoting the fluid domain around each  $G_i$  as  $F_i$ , the forward mappings  $f_i$  and inverse mappings  $g_i$  between annuli  $A_i$  and original domains  $F_i$  were computed using a set of Python bindings written for a modified version of the `DSCPACK` code by Hu (1998). Each  $A_i$  has an outer radius of 1.0 and a geometry-specific inner radius  $r_i$ . This process maps the boundary of the geometry  $G_i$  to the inner ring of the annulus, while the outer boundary of the domain  $F_i$  is mapped to the outer ring.

Using  $w$  and  $z$  to refer to complex coordinates in  $A_i$  and  $F_i$  respectively,  $64 \times 256$  grid points, equispaced in the radial and angular directions respectively, with coordinates  $\mathbf{w}_{A,i}$  were mapped to the original domains to obtain  $\mathbf{z}_{A,i} = f(\mathbf{w}_{A,i})$ . The velocity fields  $\mathbf{u}_{r,i}, \mathbf{v}_{r,i}$  for snapshots  $t \in [0, 600]$  of each  $G_i$  were used to obtain vorticity fields  $\omega_{r,i}$ . Finally,  $\mathbf{u}_{r,i}, \mathbf{v}_{r,i}, \omega_{r,i}$  plus the pressure fields  $\mathbf{p}_{r,i}$  were interpolated to  $\mathbf{z}_{A,i}$  to obtain  $\tilde{\mathbf{u}}_{r,i}, \tilde{\mathbf{v}}_{r,i}, \tilde{\omega}_{r,i}$  and  $\tilde{\mathbf{p}}_{r,i}$ , which constitute the target values of our 'Annular Sampling' dataset. This strategy is compared against a 'Cartesian Sampling' dataset, composed of ground truth values interpolated to a regular  $128 \times 128$  Cartesian grid within the domain.

The corresponding inputs are vectors  $s_{t,i}$  of sparse pressure and velocity measurements. The former are placed on object surfaces and the latter are arranged in a grid behind the objects. Based on this general template, two setups with varying sensor quantities were considered; a large setup with 50 pressure and 25 velocity (50P+25V) sensors, and a small 12P+4V setup.

Two classes of experiments were conducted using this dataset; spatial multi-geometry flow reconstruction (SMGFR) whereby the model is expected to reconstruct a target field  $\tilde{z}_{t,i}$  given  $s_{t,i}$ , and spatiotemporal MGFR (STMGFR) which is similar to SMGFR the target field is  $k$  timesteps in the future relative to the sensor input - e.g. reconstruct  $\tilde{z}_{t+k,i}$  given  $s_{t,i}$ .

## MODEL ARCHITECTURE AND TRAINING

For spatial reconstruction, the performance of four architectures was evaluated:

1. **Shallow Decoder (SD)**: A 3 layer multilayer perceptron (MLP) with 40 units and ReLU activations in the intermediate layers, as used in Erichson *et al.* (2020).
2. **SD-Large**: A larger SD with 4 layers, 2048 units in each layer, leaky ReLU activations and batch normalization.
3. **SD-UNet**: SD model with 512 and 2048 units in the intermediate layers, followed by a reshape operation to a 2D grid and a U-Net (Ronneberger *et al.* (2015)) model.
4. **SD-FNO**: An SD model identical to the one in the SD-UNet, followed by four FNO (Li *et al.* (2020)) layers.

In addition, the training of a further FNO model was explored, using the predictions of the above four spatial models as inputs and ground truth snapshots  $k = 0, k = 20$  and  $k = 80$  timesteps in the future relative to the inputs as the targets. In the  $k = 0$  configuration, this FNO model serves as a denoising autoencoder. The  $k = 20$  and  $k = 80$  configurations explore time-marching the full fields into the future, enabling spatio-

temporal flow reconstruction from sparse sensors, when used in conjunction with the spatial model.

All models were implemented using Tensorflow (Abadi *et al.* (2016)). Training was conducted using the Adam optimizer by Kingma & Ba (2017) with an initial learning rate of  $10^{-3}$ . The learning rate was dynamically tapered as validation loss plateaued. Number of training epochs was determined using the early stopping approach based on validation loss levels.

## RESULTS

Below, we present the results from a series of SMGFR and STMGFR experiments. First, we begin with the investigation of spatial pressure and velocity reconstruction, and subsequently present results for instantaneous drag and lift coefficient estimation using the reconstructed fields. Next, we focus on reconstruction of vorticity both in space and time, and statistically demonstrate that the prediction of vorticity in our setting presents a substantially greater challenge than the prediction of velocity and pressure.

### Spatial pressure and velocity reconstruction

We start with the investigation of spatial pressure and velocity reconstruction, to directly compare the quality of our reconstruction methodology with the results by Chen *et al.* (2021). For the sake of brevity, only the results using the SD-UNet spatial model coupled with the FNO-based denoising autoencoder are presented in this section, using the large sensor setup. Table 1 shows absolute and percentage validation error levels, averaged over the validation snapshots. Figure 2 depicts the ground truth and predicted fields for a random validation snapshot from the annular sampling dataset, alongside the corresponding percentage error field. Highest percentage errors are concentrated near the zero ground truth contours of each field, despite the absence of high concentrations of absolute errors near these areas, as the denominator in the percentage error calculation approaches zero, as further discussed in Özbay & Laizet (2022).

Table 1: Mean absolute error (MAE) and mean absolute percentage error (MAPE) levels for pressure and velocity SMGFR experiments. MAPE figures were filtered to exclude grid points exhibiting percentage errors above 200% since such high levels of percentage error are almost exclusively caused by ground truth values approaching zero, as seen in Figure 2.

	Annular sampling		Cartesian sampling	
	MAE	MAPE	MAE	MAPE
$p$	<b>0.0118</b>	<b>2.43%</b>	0.0133	3.32%
$u$	<b>0.0264</b>	<b>8.26%</b>	0.0332	11.56%
$v$	<b>0.0122</b>	<b>9.40%</b>	0.0164	15.61%

The error levels clearly display that annular sampling is capable of substantially improving the quality of reconstructions, bringing error levels below 3% and 10% for pressure and velocity respectively, and reducing absolute error levels by up to 25% in the case of  $v$ -velocity.

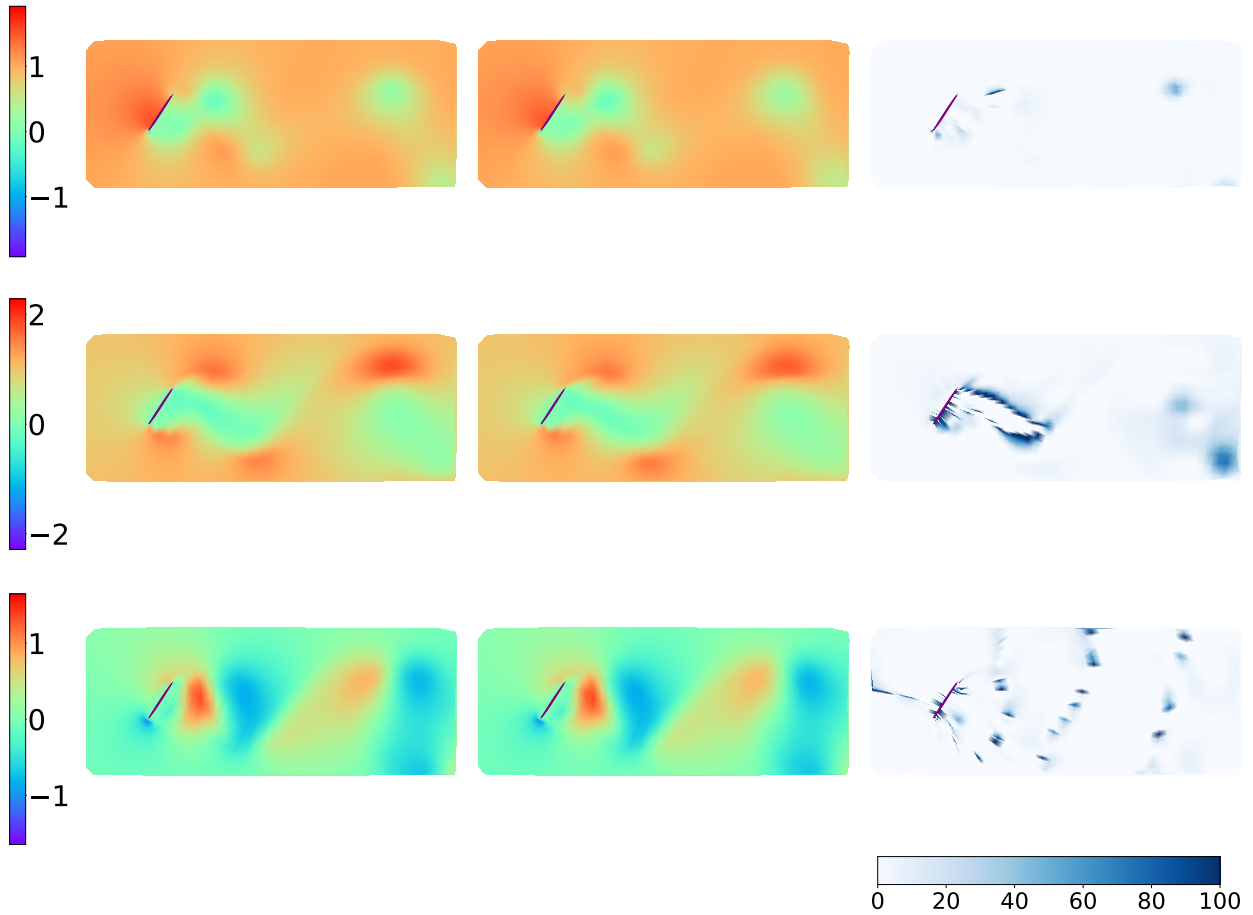


Figure 2: Ground truth (left), predicted (middle) and percentage error (right) plots for pressure (top),  $u$ -velocity (middle) and  $v$ -velocity (bottom) reconstruction for a validation snapshot.

**Lift and drag coefficient estimation** Reconstructions of pressure and velocity, when used together, can be utilized to estimate the instantaneous lift and drag coefficients. To achieve this, we adopt a strategy on the computation of body forces. Table 2 compares the errors in lift and drag coefficient derived from the Annular and Cartesian sampling methods relative to those obtained from ground truth data. Figure 3 depicts the time evolution of predicted and ground truth lift and drag coefficients for a validation geometry when using annulus sampling.

Table 2: Mean absolute error (MAE) and mean absolute percentage error (MAPE) levels for pressure and velocity SMGFR experiments

	Annular sampling		Cartesian sampling	
	MAE	MAPE	MAE	MAPE
$C_L$	<b>0.0253</b>	<b>4.97%</b>	0.0966	28.18%
$C_D$	<b>0.0214</b>	<b>8.57%</b>	0.0684	29.67%

Unlike the Cartesian sampling method, the annular sampling method allows for the computation of the forces without

the need for interpolation. This enables the estimation of lift and drag with an accuracy level comparable to the results by Chen *et al.* (2021), who reported percentage errors on the order of 3-4%. The similar levels of performance with our method is despite the order-of-magnitude larger Reynolds number and the presence of unsteady flow in the present study.

### Spatial vorticity reconstruction

To push the boundaries in multi-geometry flow reconstruction, in addition to the pressure and velocity results in the previous chapter, we detail the results of vorticity-based SMGFR tasks. Reconstruction of vorticity from pressure and velocity sensors presents a substantially greater challenge, as the reconstruction relationship relating pressure and velocity sensors to vorticity is more difficult to model, as explored further on. This creates larger differences between the best and worst performing configurations, and paints a clearer picture regarding the effect of the three variables controlled for in our study: sensor setups, model architectures and sampling strategies. Table 3 summarizes the percentage errors from the SMGFR investigations with all configurations. In this table, in addition to the standard mean absolute percentage error (MAPE), we further provide the high vorticity MAPE (HVM) metric, which is MAPE filtered such that grid points which correspond to ground truth vorticity values with magnitudes below 1% of the maximum vorticity in each snapshot are removed. This metric better represents the models' performance

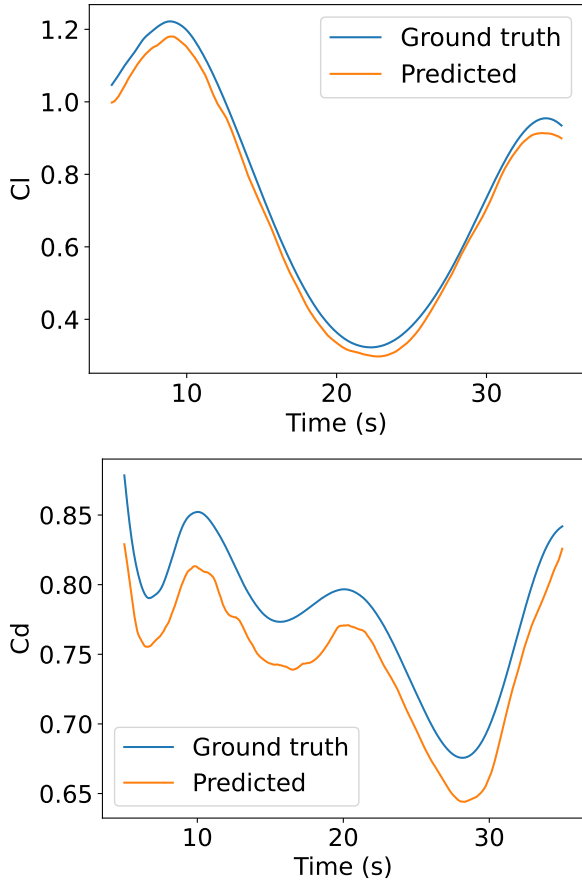


Figure 3: Time evolution of the predicted and ground truth lift (top) and drag (bottom) coefficients for a validation geometry.

in regions of interest within the flow, where the vortex shedding dynamics are observed.

The results show a clear trend regarding the relative importance of the three experimental variables; the sampling strategy permits the improvements in performance, providing an accuracy benefit exceeding 15 percentage points in the case of the SD model with the large sensor setup. Relative to this, the improvements afforded by the choice of model architecture and sensor setup are modest. The best overall-performing configuration is the SD-UNet coupled with annular sampling and the large sensor setup. Figure 4 depicts vorticity predictions with this configuration; as also covered in Özbay & Laizet (2022), our method correctly replicates flow features of interest such as the intensity and placement of shed vortices and concentrations of vorticity in boundary layers, while concentrations of high percentage error are once again observed mostly in areas where the ground truth values approach zero.

### Spatio-temporal vorticity reconstruction

Finally, we extend the results from vorticity-based SMGFR efforts to STMGFR (reconstruction in both time and space). The outputs from a spatial reconstruction model, chosen as the SD-UNet trained on the annular dataset for displaying the highest performance in SMGFR, are provided as inputs to an FNO model which is optimized to reconstruct the ground truth snapshots a fixed number of timesteps  $k$  in the future relative to its input. This allows the combined SD-UNet + FNO system to predict snapshots in the future, given current

Table 3: Percentage error metrics from the vorticity-based SMGFR experiments.

		Large sensor setup		Small sensor setup	
Sampling		Ann.	Cart.	Ann.	Cart.
SD	MAPE	44.29%	59.88%	47.35%	57.40%
	HVM	34.28%	46.14%	34.72%	50.89%
SD-Large	MAPE	43.80%	57.52%	47.20%	59.77%
	HVM	31.85%	53.36%	34.06%	48.59%
SD-UNet	MAPE	39.92%	47.64%	45.03%	51.56%
	HVM	31.37%	39.88%	33.17%	44.47%
SD-FNO	MAPE	40.83%	46.56%	44.04%	51.81%
	HVM	31.78%	39.34%	33.77%	45.81%

sensor readings. Table 4 summarizes the percentage error metrics obtained from this setup with varying values of the temporal gap  $k$ , while Figure 5 depicts the results obtained from the STMGFR procedure for the same snapshot in Figure 2.

The results clearly display that our setup is capable of predicting vorticity snapshots in the future from current sensor measurements with minimal penalties incurred in terms of accuracy.

Table 4: Percentage error metrics for the vorticity-based STMGFR task with varying temporal gaps.

$k$ ( $\Delta\tau^*$ )	0 (0.0)	20 (0.667)	80 (2.667)
MAPE	28.89%	31.02%	31.88%
HVM	17.86%	17.86%	21.97%

### Difficulties in predicting vorticity

Our method permits predictions of pressure and velocity with error levels largely in line with previous literature despite the greater challenge of tackling unsteady flows at much higher Reynolds numbers. However, much higher percentage error levels are encountered in the previously unexplored task of vorticity reconstruction around arbitrary geometries. An intuitive explanation for this is the fact that we use pressure and velocity sensors to reconstruct a third, different target field.

To test this hypothesis, we constructed two metrics to compare the difficulties of reconstructing pressure,  $u$ -velocity,  $v$ -velocity and vorticity fields given the sensor inputs from the large sensor setup. The first,  $\mathcal{D}$ , is based on the Spearman rank correlation coefficient (SRCC), which quantifies the monotonicity of the relationship between two quantities. The second,  $\mathcal{M}$ , is based on mutual information (MI), which compares the similarity (relative entropy) of the distributions of two random variables. The scores are computed by constructing matrices containing the SRCC or MI between each sensor

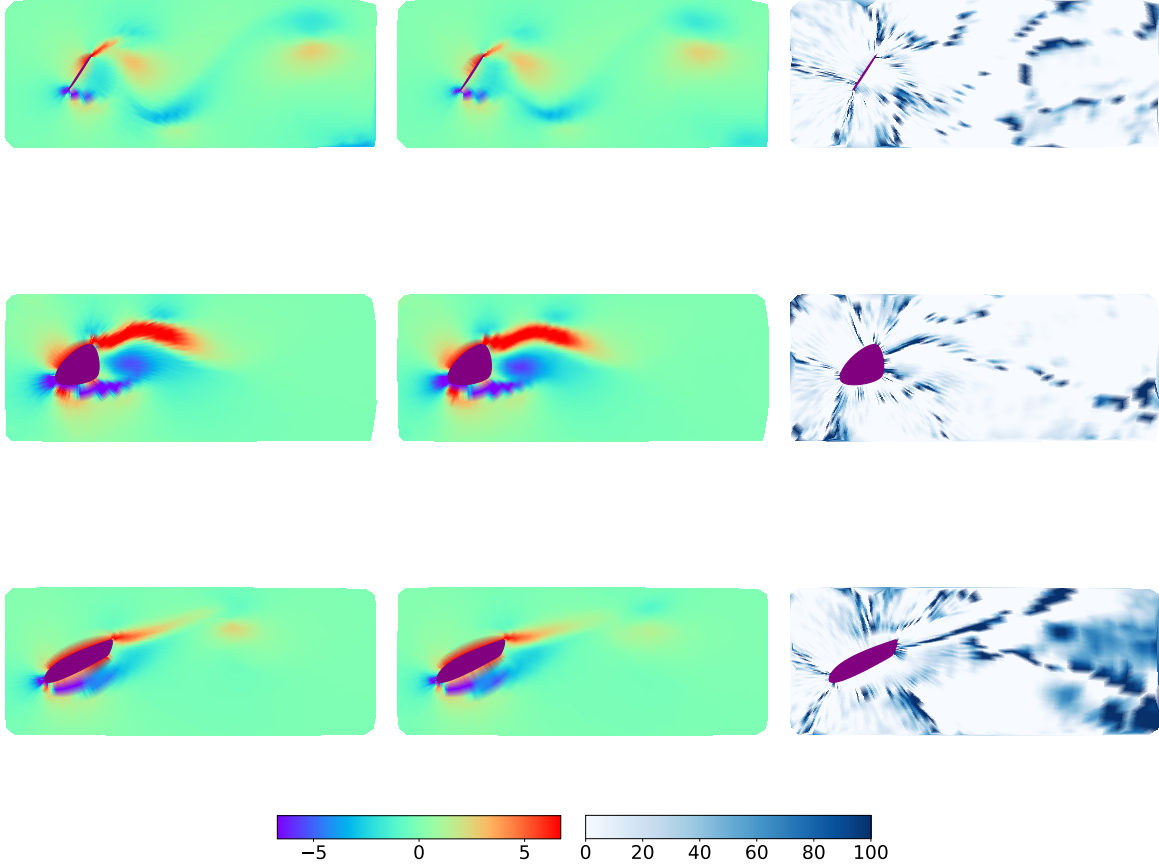


Figure 4: Ground truth (left), predicted (middle) and percentage error (right) plots for vorticity reconstructions of three validation snapshots.

input and each grid point in the target fields, and then subsequently computing the Frobenius norm of this matrix. Table 5 shows both difficulty metrics for the four target fields investigated in this study.

Table 5: Difficulty metrics  $\mathcal{D}$  and  $\mathcal{M}$  for the four target fields investigated. Higher is easier.

Variable	$p$	$u$	$v$	$\omega$
$\mathcal{D}$	306.22	298.99	301.85	242.82
$\mathcal{M}$	302.72	296.37	269.81	207.75

The difficulty metrics clearly support the hypothesis that a more difficult to learn relationship exists between the sensor inputs and vorticity compared to pressure and velocity, explaining the greater error encountered in vorticity experiments.

## CONCLUSION

We investigated the performance of NN architectures inspired by Erichson *et al.* (2020) on a flow reconstruction task involving a snapshots from a large number of randomly generated geometries. We found that the performance of such

models on this task is poor, and developed an approach for sampling the flow fields in a novel manner using Schwarz-Christoffel mappings. Comparing the performance of models trained using this sampling method versus the traditional Cartesian approach, we found that our method reduces validation errors substantially, enabling the reconstruction of pressure, velocity and vorticity with percentage errors below 3%, 10% and 30% respectively, as detailed in Özbay & Laizet (2022).

Subsequently, we used the mapping strategy to accurately predict instantaneous lift and drag coefficients, achieving percentage errors below 5% and 10% for lift and drag estimation respectively, compared to errors above 25% when using Cartesian sampling. Finally, we extended the spatial-only reconstruction task to obtain flow fields in the future relative to the sensor measurements, reconstructing vorticity fields in the future with minimal error increases compared to contemporaneous predictions.

In the future, we aim to extend this work by exploring reconstruction in 3D with varying Reynolds numbers.

## REFERENCES

Abadi, Martín, Barham, Paul, Chen, Jianmin, Chen, Zhifeng, Davis, Andy, Dean, Jeffrey, Devin, Matthieu, Ghemawat, Sanjay, Irving, Geoffrey, Isard, Michael *et al.* 2016 Tensorflow: A system for large-scale machine learning. In *12th*

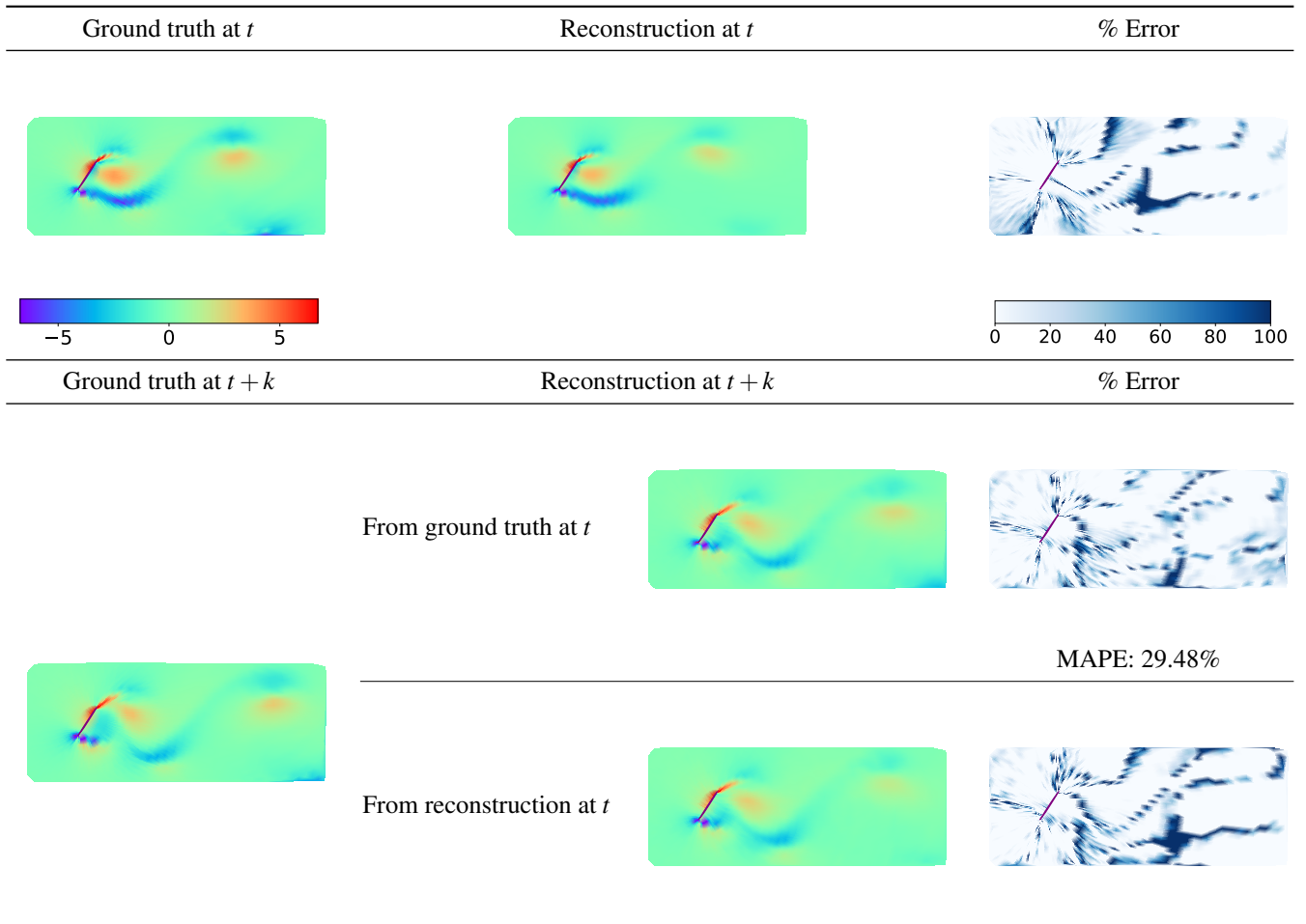


Figure 5: Ground truth (left), reconstructed vorticity fields (middle) and percentage error fields (right) for the STMGFR task, conducted on the same geometry as in Figure 2. The top row displays purely spatial reconstruction at timestep  $t$  with the SD-UNet, while the bottom rows display the predictions from the FNO model for the vorticity field at timestep  $t+k$ .

{USENIX} symposium on operating systems design and implementation ({OSDI} 16), pp. 265–283.

Bonnet, Jean P, Cole, Daniel R, Delville, Joël, Glauser, Mark N & Ukeiley, Lawrence S 1994 Stochastic estimation and proper orthogonal decomposition: complementary techniques for identifying structure. *Experiments in fluids* **17** (5), 307–314.

Callaham, Jared L., Maeda, Kazuki & Brunton, Steven L. 2019 Robust flow reconstruction from limited measurements via sparse representation. *Phys. Rev. Fluids* **4**, 103907.

Chen, J., Hachem, E. & Viquerat, J. 2021 Graph neural networks for laminar flow prediction around random two-dimensional shapes. *Physics of Fluids* **33** (12), 123607.

Crowdy, Darren 2020 *Solving problems in multiply connected domains*. SIAM.

Dubois, Pierre, Gomez, Thomas, Planckaert, Laurent & Perret, Laurent 2022 Machine learning for fluid flow reconstruction from limited measurements. *Journal of Computational Physics* **448**, 110733.

Erichson, N. Benjamin, Mathelin, Lionel, Yao, Zhewei, Brunton, Steven L., Mahoney, Michael W. & Kutz, J. Nathan 2020 Shallow neural networks for fluid flow reconstruction with limited sensors. *Proceedings of the Royal Society A: Mathematical, Physical and Engineering Sciences* **476** (2238), 20200097.

Hu, Chenglie 1998 Algorithm 785: A software package for computing schwarz-christoffel conformal transformation for doubly connected polygonal regions. *ACM Trans. Math. Softw.* **24** (3), 317–333.

Kingma, Diederik P. & Ba, Jimmy 2017 Adam: A method for stochastic optimization.

Li, Zongyi, Kovachki, Nikola, Aizzadenesheli, Kamyar, Liu, Burigede, Bhattacharya, Kaushik, Stuart, Andrew & Anandkumar, Anima 2020 Fourier neural operator for parametric partial differential equations. *arXiv preprint arXiv:2010.08895*.

Özbay, Ali Girayhan & Laizet, Sylvain 2022 Deep learning fluid flow reconstruction around arbitrary two-dimensional objects from sparse sensors using conformal mappings. *AIP Advances* **12** (4), 045126.

Ronneberger, Olaf, Fischer, Philipp & Brox, Thomas 2015 U-net: Convolutional networks for biomedical image segmentation. In *International Conference on Medical image computing and computer-assisted intervention*, pp. 234–241. Springer.

Viquerat, Jonathan, Rabault, Jean, Kuhnle, Alexander, Ghraieb, Hassan, Larcher, Aurélien & Hachem, Elie 2021 Direct shape optimization through deep reinforcement learning. *Journal of Computational Physics* **428**, 110080.

Witherden, F.D., Farrington, A.M. & Vincent, P.E. 2014 Pyfr: An open source framework for solving advection–diffusion type problems on streaming architectures using the flux reconstruction approach. *Computer Physics Communications* **185** (11), 3028–3040.